https://doi.org/10.5194/egusphere-2025-91
Preprint. Discussion started: 17 February 2025

Global validation of the Particulate Observing Scanning Polarimeter (POSP) Aerosol Optical Depth products over land

Zhe Ji[1,2], Zhengqiang Li[1,2,3*], Gerrit de Leeuw[1,4], Zihan Zhang[1], Yan Ma[1], Zheng Shi[5], Cheng Fan[1], Qiao Yao[1,2]

[1] Key Laboratory of Remote Sensing and Digital Earth & Key Laboratory of Satellite Remote Sensing of Ministry of Ecology and Environment, Aerospace Information Research Institute, Chinese Academy of Sciences, Beijing 100101, China
[2] University of Chinese Academy of Sciences, Beijing 100049, China
[3] College of Remote Sensing and Geoinformatics Engineering, Faculty of Geographical Science and Engineering, Henan University, Zhengzhou 450046, China
[4] Royal Netherlands Meteorological Institute (KNMI), R & D Satellite Observations, 3730 AE De Bilt, The Netherlands
[5] The Administrative Center for China's Agenda 21, Beijing 100098, China

Correspondence to: Zhengqiang Li (lizq@radi.ac.cn)

Abstract. The global AODs for the one of few single-angle polarimeters currently in orbit, Particulate Observing Scanning Polarimeter (POSP) has been proposed. We have tested the retrievals from the early stages of on-orbit operation and achieved high accuracy, but we still lack an understanding of the retrieval accuracy over longer time scales. The systematic validation and analysis of POSP retrievals are imperative to ensure the reliability of AOD products and to provide scientific references for further enhancement. To this end, POSP AOD products have been compared with Aerosol Robotic Network (AERONET) measurements at over 276 sites. The results from 19314 collocations show a high accuracy, with correlation coefficients (R) of 0.914, a root mean square error (RMSE) of 0.085, and the fraction within the expected error (EE) is 78.5%. The error analysis shows that the accuracy of POSP AOD exhibits a clear seasonal variation, being lower in the autumn and winter than in the spring and summer. Additionally, the uncertainty in AOD increases as NDVI decreases. Compared with MODIS AOD products, the accuracy of POSP AOD was higher than that of the Deep Blue product except over barren and forest, and higher than the Dark Target product over all surface types. In addition, the spatial variability characteristics of the global mean AOD has been analyzed. POSP AOD shows an underestimation compared to MODIS BD AOD over North Africa and the Arabian Peninsula, while it overestimates in other regions. However, both POSP AOD and MODIS AOD indicate that high aerosol loading mainly occurs over northern South America, central Africa, northern India, and northeastern China.

1 Introduction

Aerosols consist of particulate matter (referred to as particles) suspended in the atmospheric fluid. Aerosols have increasingly attracted attention because of the air pollution caused by the rise in global industrial activity brought about by economic growth in recent years (Wei et al., 2023) and other anthropogenic activities such as transportation and generation of energy. Due to the large variation of sources, atmospheric aerosols have a wide variety of effects (de Leeuw et al., 2011). One of the most

https://doi.org/10.5194/egusphere-2025-91
Preprint. Discussion started: 17 February 2025

notable effects is the direct impact of aerosols on atmospheric radiation (Stocker et al., 2013). Aerosol particles scatter solar radiation thus reducing the amount of radiation that reaches the Earth' surface, thereby causing a cooling effect. In contrast, absorbing aerosols can absorb solar radiation, leading to a local warming effect (Guo et al., 2016). Aerosol particles can also act as cloud condensation nuclei (CCN) which in high relative humidity conditions can be activated and grow into cloud droplets. By influencing the CCN, aerosol particles can indirectly alter the microphysical properties of clouds (Bellouin et al., 2020; Liu et al., 2022; Myhre et al., 2007; Rosenfeld et al., 2014). Both effects depend both on the size of the aerosol particles and on their composition. However, the composition of aerosol particles is extremely complex, and there is currently a lack of clarity of perception on the distribution of aerosol composition (Chen et al., 2022). As a consequence, the Intergovernmental Panel on Climate Change (IPCC) still considers aerosols to be one of the largest sources of uncertainty in global warming (Lee et al., 2023). In addition to their impact on atmospheric processes affecting climate, aerosols affect air quality with harmful effects on, for instance, human health (He and Huang, 2018; Li et al., 2017b). The inhalation of aerosol particles into the human body results in accumulation in the respiratory system where they can cause various diseases (Rosenfeld, 2000). At the same time, high concentrations of aerosols significantly reduce near-surface visibility, crop production, etc.

Traditionally, the study of aerosol properties has mainly relied on ground-based observations. Through long-term investments and developments by various countries and their research institutions, a large number of ground-based observation sites have been established, providing optical and microphysical aerosol properties in key research areas (Dubovik et al., 2002; Levy et al., 2007). Examples include NASA's AErosol RObotic NETwork (AERONET) (Holben et al., 1998), Europe's PHOtométrie pour le Traitement Opérationnel de Normalisation Satellitaire (PHOTONS) (Goloub et al., 2008), China's Sun–sky radiometer Observation NETwork (SONET) (Li et al., 2018b), the China Aerosol Remote Sensing NETwork (CARSNET) (Che et al., 2015) and so on. In addition to these ground-based remote sensing activities, a wide variety of ground-based in situ networks has also been established on global (Moreno, 2023; Yuba et al., 2023), continental (Tørseth et al., 2012) and national (Bai et al., 2020; Beig et al., 2021; Cobourn, 2007; Hoff et al., 2006; Wu et al., 2018) scales. However, ground-based observations cannot provide data on global or regional spatial scales and lack coverage in areas with humanly inaccessible areas. This gap can be filled by satellite observations, providing characterization of aerosols on regional to global scales, but with the lower accuracy. From the perspective of sustainable development, the Chinese government has actively responded to the call for global environmental governance by launching numerous satellites for atmospheric environment monitoring (Liangfu et al., 2021; Wang et al., 2021; Xian et al., 2021; Zhao et al., 2017). Among these, the Particulate Observation Scanning Polarimeter (POSP), mounted on the Gaofen-5(02) satellite, was successfully launched in July 2021. POSP is a single-view multispectral polarimeter with a nadir resolution of 6.4 km.

Aerosol Optical Depth (AOD) is the primary parameter used to assess the atmospheric aerosol content. It is a key parameter for evaluating the aerosol monitoring capability of satellites. Observations from POSP provide valuable information for the retrieval of aerosol properties (Li et al., 2022). An aerosol retrieval algorithm for application to POSP was initially developed by Shi et al. (2023), that reconstructed the surface reflectance of POSP for aerosol retrieval. Then, Ji et al. (2025) proposed a more accurate aerosol algorithm that takes into account the directional properties of the surface. By exploring the empirical

https://doi.org/10.5194/egusphere-2025-91
Preprint. Discussion started: 17 February 2025

relationships between adjacent blue bands, the new algorithm has realized the joint inversion of multiple blue bands. An optimization algorithm also has been used to incorporate boundary constraints which simultaneously accounts for errors in the surface constraint, and the satellite observations. Thus, POSP AOD products are successfully retrieved with high precision. Initial evaluation of the AOD products retrieved with this updated algorithm by comparison with MODIS data during the period November 2021 to April 2022 shows the better performance of the enhanced POSP aerosol algorithm. However, an understanding of the accuracy of the algorithm over a longer time and for different seasons and surface types is still lacking. To further validate the accuracy of the POSP AOD product and to identify the direction of further improvement, we validated the AOD product for a longer time series from December 2021 to November 2022.Comparisons of POSP AOD with AERONET AOD shows a high degree of consistency, and its accuracy surpasses that of MODIS AOD for the same time period (Ji et al., 2025). In this study, we first evaluate the accuracy of POSP AOD retrievals on seasonal, regional, and local scales using AOD from 276 AERONET sites across the world. The POSP products are also cross-validated with AOD from MODIS/Terra, which has a similar equator crossing time as POSP. This study is dedicated to a comprehensive and accurate evaluation of POSP AOD products, delving into the exploration of potential factors influencing their performance. The ultimate goal is to provide a valuable reference for the enhancement of these products in future iterations.

2 Material

2.1 POSP AOD products

The Particulate Observation Scanning Polarimeter (POSP), a state-of-the-art polarimeter on board the GF-5(02) satellite. It has a field of view of ±50° with a swath width of ~1850 km, provides global observations in nine spectral bands spanning wavelengths from 380 to 2250 nm (Lei et al., 2023). An enhanced general aerosol algorithm has been developed to retrieve AOD using POSP data (Ji et al., 2025). In this algorithm, by employing a non-Lambertian radiative transfer model and leveraging surface constraints established using MODIS BRDF products (MCD43), we achieved high-precision AOD retrieval. POSP AOD has the same resolution as POSP observations (6.4 km). Relying on the high-precision calibration results of POSP (the intensity observation error is within 5%, and the degree of linear polarization error is better than 0.005). In previous study, our enhanced algorithm demonstrates the potential to retrieve high-accuracy aerosol products and has shown very high precision in preliminary testing (from November 2021 to April 2022) (Ji et al., 2025).

2.2 MODIS products

The MODIS AOD product has been operational for many years and has demonstrated stability through extensive validation (Levy et al., 2013; Sayer et al., 2013). Thanks to the efforts of the MODIS team, the accuracy of these products has not declined over time. In this study, we selected the Level 2.0 (L2) MODIS/Terra Deep Blue and Dark Target (MOD04) AOD products with a spatial resolution of 10 km, for comparison. Furthermore, the MODIS AOD products have quality flags (QA), with

https://doi.org/10.5194/egusphere-2025-91
Preprint. Discussion started: 17 February 2025

QA=3 representing the highest quality. In the cross-validation with MODIS, we only used data with QA=3 during the comparison process.

To quantitatively assess the accuracy performance of the POSP AOD algorithm across different surface types, the land cover product MCD12Q1 (2022) (Sulla-Menashe and Friedl, 2018), with a spatial resolution of 500 meters was used in this study. The International Geosphere-Biosphere Programme (IGBP) classification scheme was applied, which has been widely used in climate and environmental studies as a global classification standard for describing land cover types, especially in the classification and interpretation of Earth observation satellite data. The global IGBP classification results for 2022 are depicted in Fig.1. To match the POSP window size, the MCD12Q1 was resampled to 0.005°×0.005°. Subsequently, within a 40×40 window centered on the pixels containing the site location, the highest occurrence within this window was selected as the representative classification for the site (MODIS products are available from https://ladsweb.modaps.eosdis.nasa.gov/).

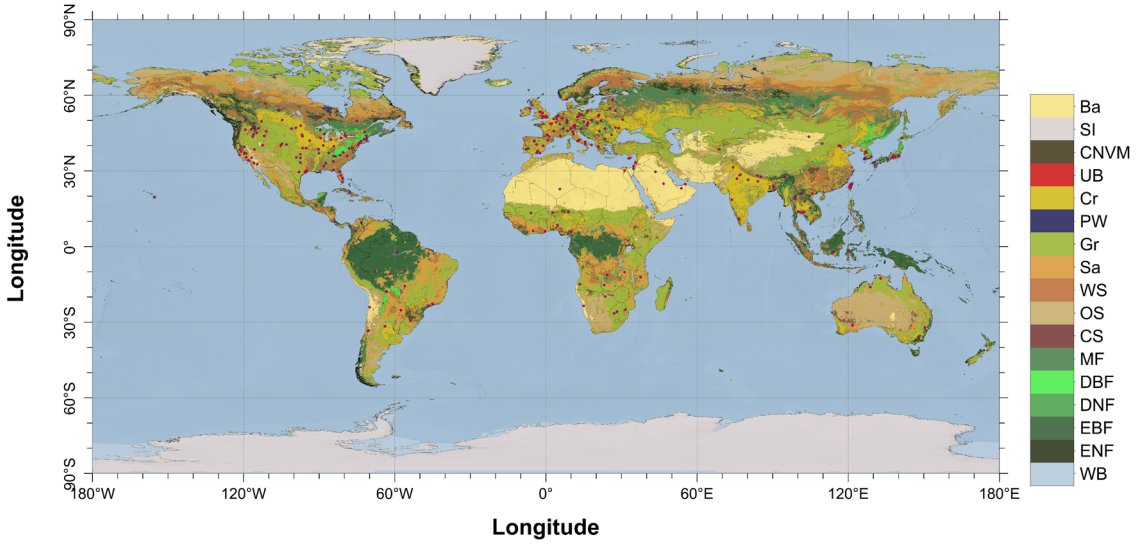

Figure 1: The distribution of selected AERONET sites globally. The red points represent inland sites. The background is the MCD12C1 classification result (IGBP) in 2022 (WB: Water Bodies; ENF: Evergreen Needleleaf Forests; EBF: Evergreen Broadleaf Forests; DNF: Deciduous Needleleaf Forests; DBF: Deciduous Broadleaf Forests; MF: Mixed Forests; CS: Closed Shrubland; OS: Open Shrublands; WS: Woody Savannas; Sa: Savannas; Gr: Grasslands; PW: Permanent Wetlands; Cr: Croplands; UB: Urban and Built up Lands; CNVM: Cropland Natural Vegetation Mosaics; SI: Permanent Snow and Ice; Ba: Barren).

2.3 AERONET data

AERONET provides aerosol products with low uncertainties with 0.01 in the VIS range and 0.02 in the UV range (Eck et al., 1999; Giles et al., 2019), and has been extensively used for validation (Chu et al., 2002; He et al., 2016; Levy et al., 2010; Sayer et al., 2013; Xie et al., 2019; Che et al., 2016). AERONET V3 provides AOD datasets at three distinct quality levels: Level 1.0 following pre-screening, Level 1.5 after cloud identification and instrument anomaly monitoring, and Level 2.0 after cloud identification, instrument anomaly monitoring, and quality control screening (https://aeronet.gsfc.nasa.gov/). In this study, Level 1.5 data is chosen as the ground-based validation data to minimize validation errors.

https://doi.org/10.5194/egusphere-2025-91
Preprint. Discussion started: 17 February 2025

Since POSP AOD products are produced at 550 nm, it is necessary to interpolate AOD data obtained from AERONET observations to match this wavelength. This interpolation is performed using the Ångström Exponent (AE) (Ångström, 1929).

$$\tau_\lambda = \beta\lambda^{-\alpha}, \quad (1)$$

where λ is the specified wavelength in microns, τ_λ is the AOD at the specified wavelength, and α is the Ångström Exponent (AE), the value of which characterizes the aerosol particle size.

The POSP AOD algorithm is only applicable to land and cannot provide aerosol data over ocean and coastal regions. In this study, stations within a 20 km buffer zone from the coastline are defined as coastal stations and they are excluded to ensure reliability of the results, which leaves 276 remaining sites.

3 Methods

3.1 Matching strategy

Various spatial and temporal matchup strategies applicable to different satellite aerosol products have been proposed (Chu et al., 2002; Ichoku et al., 2002; Sayer et al., 2013; Virtanen et al., 2018). In this study, considering the 6.4 km spatial resolution of the POSP, the following matching strategies have been devised to ensure reliable AOD validation results while accounting for spatial consistency: satellite data are averaged over a 3 × 3 window centered on the AERONET site, and ground-based observations are averaged over a 30-minutes window before and after the time of satellite overpass. To mitigate the uncertainty associated with averaged data, a minimum of two or more ground-based observations are required in the temporal matching window, and the spatial matching window must encompass more than three valid satellite observation pixels (Chu et al., 2002). To facilitate accurate comparison with MODIS AOD products, we applied the same criteria to match POSP and MODIS AOD data. To investigate the influence of land cover (LC) on the POSP AOD retrieval, the validation was repeated for sub-sets of POSP data over different LC types, using the IGBP classification. Because the number of match-ups over some IGBP LC types was too small to achieve statistical significance, the data over those IGBP LC types were merged. We merged different types of forested areas into the "Forest" category and shrublands with low vegetation into the "Grassland" category. The Forest represents evergreen broadleaf forest, evergreen needleleaf forest, deciduous broadleaf forest, and mixed forest, while the Grassland represents woody savannas, grassland, and savanna. The independent validation results for each IGBP type are presented in supplementary.

3.2 Statistical metrics

To quantitatively assess the accuracy of the retrieval results and the applicability of the retrieval algorithms over different land cover conditions, statistical metrics were calculated for the comparison between the matched AOD data pairs. These metrics include the Pearson correlation coefficient (R), which reflects the degree of agreement between the ground-based observations and the satellite retrieval results.

https://doi.org/10.5194/egusphere-2025-91
Preprint. Discussion started: 17 February 2025

$$R = \frac{\sum_{i=1}^{n}\left(AOD_{AERONET,i}-\overline{AOD_{AERONET}}\right)\left(AOD_{Satellite,i}-\overline{AOD_{Satellite}}\right)}{\sqrt{\sum_{i=1}^{n}\left(AOD_{AERONET,i}-\overline{AOD_{AERONET}}\right)^2 \sum_{i=1}^{n}\left(AOD_{Satellite,i}-\overline{AOD_{Satellite}}\right)^2}}, \quad (2)$$

where $AOD_{AERONET,i}$ denotes the AERONET reference data, $AOD_{Satellite,i}$ denotes the satellite retrieval data, n denotes the number of matched data pairs, and $\overline{AOD_{AERONET}}$ and $\overline{AOD_{Satellite}}$ denote the averages of each of these parameters, which represents the overall trend of the ground-based and satellite-based AOD data, respectively.

R^2 (R-squared), also known as the coefficient of determination, represents the difference between the satellite retrievals and the ground-based retrievals. Its value ranges from 0 to 1, with values closer to 1 indicating the difference between them is quietly small, and values closer to 0 indicating the difference between them is large.

$$R^2 = 1 - \frac{\sum_{i=1}^{n}\left(AOD_{AERONET,i}-AOD_{Satellite}\right)^2}{\sum_{i=1}^{n}\left(AOD_{AERONET,i}-\overline{AOD_{AERONET}}\right)^2}, \quad (3)$$

Root Mean Square Error (RMSE), which represents the uncertainty in the results of ground-based observations and satellite inversions.

$$RMSE = \sqrt{\frac{1}{n}\sum_{i=1}^{n}\left(AOD_{Satellite,i} - AOD_{AERONET,i}\right)^2}, \quad (4)$$

Mean Absolute Error (MAE), which indicates the overall estimation accuracy of the algorithm.

$$MAE = \frac{1}{n}\sum_{i=1}^{n}\left|AOD_{Satellite,i} - AOD_{AERONET,i}\right|, \quad (5)$$

Bias, is a measure of underestimation or overestimation with respect to the reference data.

$$Bias = \frac{1}{n}\sum_{i=1}^{n} AOD_{Satellite,i} - AOD_{AERONET,i}, \quad (6)$$

Furthermore, the quality of the AOD retrieval results is assessed in this study using a combination of absolute and relative errors, referred to as the expected error (EE). EE represents the average expected level of the AOD product globally, containing at least 67% (approximately one standard deviation) of the matches should fall (Levy et al., 2013; Xie et al., 2019). In this study we adopt the EE which applies to the MODIS Collection 6 (C6.1) AOD data set, enabling a comparison of accuracy with MODIS AOD products under the same criteria (Levy et al., 2010, 2013):

$$EE = \pm(0.05 + 0.15 * AOD_{AERONET}), \quad (7)$$

We also implemented more rigorous criteria proposed by the Global Climate Observing System (GCOS), which have been adopted in the Aerosol_cci study (Chen et al., 2020; Popp et al., 2016; Secretariat, 2006).

$$GCOS = maximum(0.03, 0.1 \times AOD_{AERONET}), \quad (8)$$

https://doi.org/10.5194/egusphere-2025-91
Preprint. Discussion started: 17 February 2025

4 Results

4.1 Overall validation

Fig. 2 (A) provides an overall comparison of POSP AOD in 2022 against AERONET AOD. The figure shows the good comparison between POSP AOD and AERONET, with R of 0.914, R^2 of 0.825, RMSE of 0.086, MAE of 0.054, and Bias of 0.002. There are 19,314 match-ups for POSP, the fraction within EE is 78.45% and the fraction within GCOS is 48.6%.

The probability density functions of differences (POSP-AERONET) in Fig. 2 (B), for different AOD intervals as indicated by the different colors, show that the POSP algorithm underestimates the AOD as AOD increases. For low AOD (AOD < 0.2), POSP's bias is 0.01. For moderate AOD (0.2 ≤ AOD ≤ 0.7), POSP's bias increases to -0.03 and when AOD > 0.7, POSP's bias further increases to -0.04. The accuracy of POSP AOD decreases at high AOD, which may be attributed to the increasing aerosol model error. As AOD increases, the impact of discrepancies between the assumed aerosol model and the actual aerosol model is amplified, leading to an increase in retrieval uncertainty (Hou et al., 2018; Li et al., 2018a). Box plots of differences between POSP and AERONET AOD against AERONET AOD in Fig. 2 (C) show how the AOD bias is distributed across different AOD intervals. With the increase in aerosol loading, the AOD bias overall decreases but exhibits an anomaly at high AOD, spiking from negative to positive values. Except for the aerosol model error, the possible reason for this anomaly is because the frequency of high AOD decreases with increasing AOD, and the smaller statistical sample introduces a greater uncertainty, so in order to obtain more definitive conclusions about when high AOD is present, we will discuss the results of a longer period of time in future research.

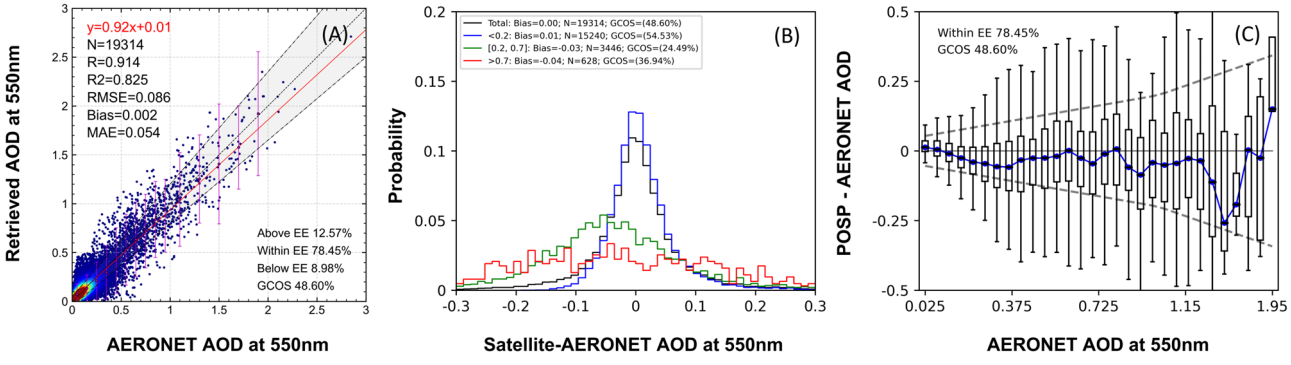

Figure 2: (A) Scatter density plot of POSP AOD versus AERONET AOD, where N—number of collocated data pairs, R—Pearson correlation coefficient, RMSE—root mean square error, MRE—mean relative error, and EE—data fraction within EE. The black dotted line represented the one-to-one line. The red line represents the linear regression fit, and the black dashed lines are EE lines. The magenta points are means for specific ranges of AERONET and satellite AOD, and the magenta lines are the mean ±2σ of retrievals in a certain range. (B) Probability density plot of differences (POSP-AERONET), The black, blue, green and red solid lines indicate all AOD conditions: any AOD, AOD < 0.2, 0.2 ≤ AOD ≤ 0.7 and AOD > 0.7, respectively. (C) Box plots of difference between POSP AOD and AERONET AOD against AERONET AOD.

4.2 Validation of POSP AOD in different seasons

On the one hand, Atmospheric and aerosol conditions are different across different seasons (Bergametti et al., 1989; Rabha and Saikia, 2020). On the other hand, due to the changes in land cover type and thus surface reflectance, and changes in aerosol

https://doi.org/10.5194/egusphere-2025-91
Preprint. Discussion started: 17 February 2025

properties in response to changes in aerosol sources between different seasons, the accuracy of AOD retrieval also changes between seasons (Che et al., 2016; Fan et al., 2023; He et al., 2016). Therefore, assessing the performance of AOD accuracy in different seasons is one of the important ways to evaluate aerosol algorithms. Fig.3 show that POSP AOD is more accurate in SON (September, October, November) and DJF (December, January, February) than in the MAM (March, April, May) and JJA (June, July, August). We also compared the AOD of the MODIS product (DB/DT) across different seasons and found that its accuracy in SON and DJF is significantly better than in MAM and JJA. The comparison results are presented in Figs. S2 and S3. The comparisons of POSP AOD versus AERONET reference data (similar to Fig.2) for different seasons shows that POSP AOD has the highest accuracy in DJF, with R of 0.932, R^2 of 0.864, RMSE of 0.08, MAE of 0.048, the fraction within EE (%EE) is 82.13%, and the fraction within GCOS is 54.38%. These metrics are better than in other seasons, with SON the second best, with R of 0.930, R^2 of 0.855, RMSE of 0.083, MAE of 0.052, the fraction within EE is 79.85%, and the fraction within GCOS is 51.94%. JJA has the lowest accuracy, with R of 0.838, R^2 of 0.667, RMSE of 0.083, MAE of 0.055, the fraction within EE is 75.98% and the fraction within GCOS is 44.17%. The bias is very small in all seasons with a largest value of 0.005 in MMA. The higher accuracy of both POSP AOD and MODIS AOD during DJF and SON compared to MAM and JJA may be attributed to the fact that most of the AERONET sites used for validation are located in the Northern Hemisphere (in Fig. 1). DJF and SON correspond to winter in the Northern Hemisphere, a period when surface changes are slower, and sudden pollution events are less frequent. As a result, the empirical constraints used in the retrieval process are more effective compared to those applied during the summer, when surface changes occur more rapidly. However, the coverage is smallest in the DJF (N=3834) and highest in the JJA (N=5454) with SON and MMA somewhat less coverage than in JJA (N=5096 and 4930, respectively). A possible reason for this is that DJF corresponds to winter in the Northern Hemisphere, during which snow and ice cover significantly reduce the satellite retrieval results. Here, we use the abbreviations of the months' initials instead of the corresponding seasons because the study includes regions in both the Northern and Southern Hemispheres, where the seasons are opposite. Using seasons could cause unnecessary confusion.

https://doi.org/10.5194/egusphere-2025-91
Preprint. Discussion started: 17 February 2025

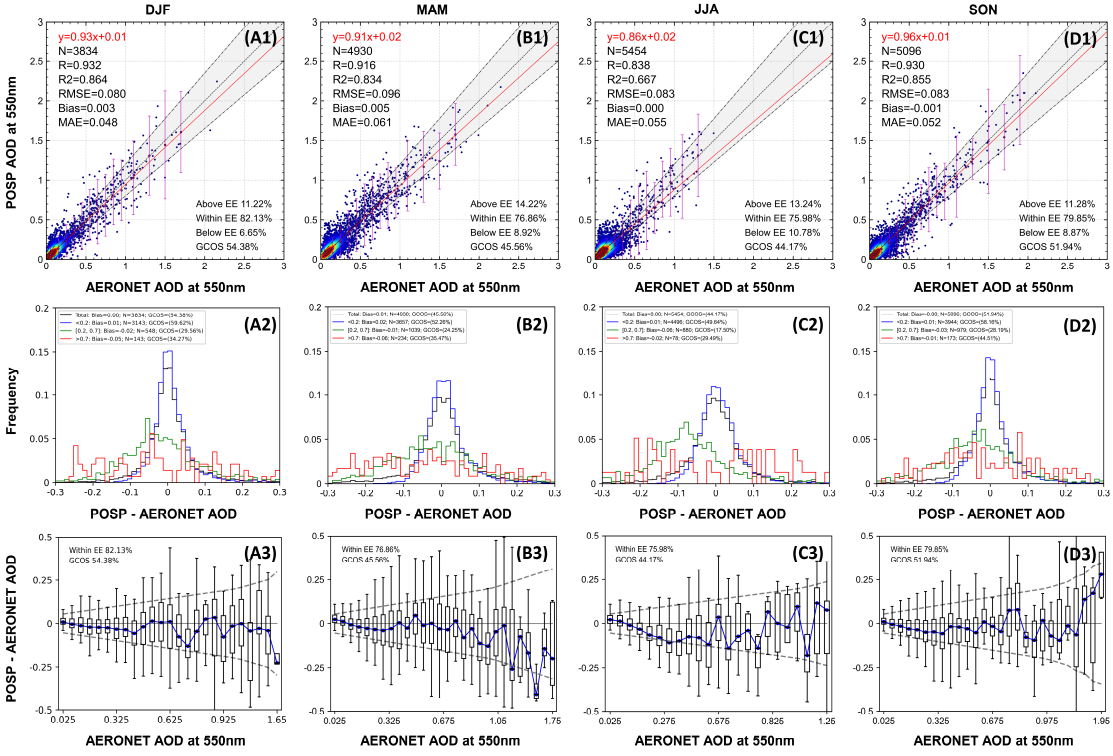

Figure 3: (1) Scatter density plots of POSP AOD versus AERONET AOD for different seasons: winter, spring, summer and autumn (columns A, B, C and D). (2) The probability density functions of differences (POSP-AERONET), The black, blue, green and red solid lines indicate all AOD conditions: any AOD, AOD < 0.2, 0.2 ≤ AOD ≤ 0.7 and AOD > 0.7, respectively. (3) Box plots of difference between POSP AOD and AERONET AOD against AERONET AOD, in (A) DJF, (B) MAM, (C) JJA, and (D) SON. The black dots and error bars represent the median, 25th percentiles, and 75th percentiles of the AOD bias.

4.3 Validation of POSP AOD in different surface types

Kaufman et al. (1997) pointed out that a small error of 0.01 in surface reflectance can lead to a 0.1 increase in AOD uncertainty. However, surface reflectance varies considerably at different surface types, so the accuracy of retrievals may vary with surface type, necessitating further in-depth analysis. Fig.4 shows the validation results of POSP AOD over four different groups of land cover types: city, cropland, grassland, and forest. It is challenging to determine which POSP AOD in land cover type has the best accuracy based on a single accuracy metric. Although Forest has the lowest RMSE and the highest fraction within the EE (79.92%) and GCOS (51.08%), it does not necessarily have the highest accuracy since it lacks high AOD cases and has the lowest R (0.85). Considering multiple accuracy metrics, we conclude that Cropland, Grassland, and Forest have similar accuracies, while City has the lowest accuracy (in Fig. 5). Table 1 shows the validation results for more detailed IGBP LC types. The data in Table 1 show that, among the Forest types, Evergreen Needleleaf Forests have the highest accuracy. The differences between the metrics for different types of forests are substantial. However, since the matching results for Evergreen Needleleaf Forests, Evergreen Broadleaf Forests, and Mixed Forest are far fewer than for other land cover types, and the retrievals are simultaneously affected by clouds and surface estimation accuracy, we can't conclude whether the accuracy of

https://doi.org/10.5194/egusphere-2025-91
Preprint. Discussion started: 17 February 2025

POSP AOD over Evergreen Broadleaf Forests within the validation period is high or not. To explain this result further validation is required with more retrieval data in future studies. The accuracy for the grassland is relatively stable, with Woody Savannas having the highest accuracy (R of 0.937, R^2 of 0.813, RMSE of 0.081, MAE of 0.049, Bias of 0.014, the fraction within EE of 81.57%, and the fraction within GCOS of 53.33%).

Other LC types which are not shown in Fig.4 are presented in Fig. S1. Fig. S1 shows that the retrieval accuracy of POSP AOD over barren is abnormal, with a significant underestimation as the AOD increases. However, it achieves acceptable accuracy (the fraction within EE of 84.7%). The reason for this impact may be our assumption in the retrieval process that the apparent reflectance at 1610 nm is not affected by aerosols and can be approximated as surface reflectance. In reality, as aerosol particle size increases, the influence of aerosols on the apparent reflectance at 1610 nm also increases (Hsu et al., 2013). Barren, due to the absence of vegetation, is more likely to generate large aerosol particles, thereby affecting the retrieval accuracy (Ginoux et al., 2001; Tegen, 2003). Overall, compared to RMSE and fraction within EE, all types of RMSE are below 0.1, and EE% is above 70% (except for EBF). Therefore, our aerosol retrieval algorithm demonstrates the ability to achieve high-precision AOD retrieval for nearly all surface types.

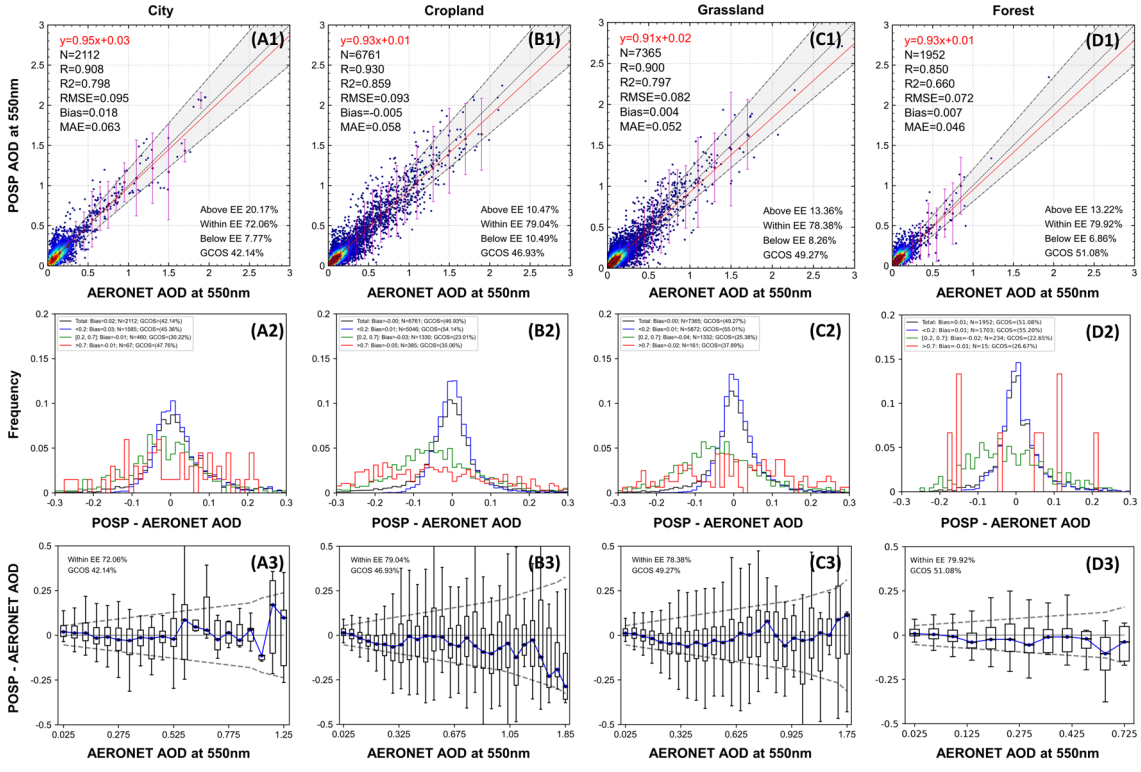

Figure 4: Same as Fig.3 but for different land cover types: (a) city, (b) Cropland, (c) grassland, and (d) forest.

https://doi.org/10.5194/egusphere-2025-91
Preprint. Discussion started: 17 February 2025

Table 1: Statistics of different algorithms in different LULC types (DBF: Deciduous Broadleaf Forests; ENF: Evergreen Needleleaf Forests; EBF: Evergreen Broadleaf Forests; Gl: Grasslands; MF: Mixed Forests; Sa: Savannas; WS: Woody Savannas; UB: urban; Ba: Barren; Cl: Croplands;).

	DBF	EBF	ENF	MF	Gl	Sa	WS	UB	Cl	Ba
N	1036	223	242	451	4000	2090	1275	2112	6761	1124
R	0.811	0.777	0.965	0.631	0.881	0.911	0.937	0.908	0.930	0.686
R2	0.565	0.569	0.885	0.176	0.776	0.814	0.813	0.798	0.859	0.442
RMSE	0.065	0.107	0.068	0.067	0.080	0.087	0.081	0.095	0.093	0.064
Bias	0.007	0.007	-0.003	0.011	-0.001	0.006	0.014	0.018	-0.005	-0.012
MAE	0.041	0.077	0.044	0.044	0.052	0.055	0.049	0.063	0.058	0.038
%EE	83.49	64.57	80.17	79.16	77.28	78.56	81.57	72.06	79.04	84.70
%GCOS	55.79	29.15	49.59	51.88	48.05	49.14	53.33	42.14	46.93	62.10

	Forest	Grassland
N	1952	7365
R	0.850	0.900
R2	0.660	0.797
RMSE	0.072	0.082
Bias	0.007	0.004
MAE	0.046	0.052
%EE	79.92	78.38
%GCOS	51.08	49.27

4.4 Site-specific validation metrics

To analyze the accuracy of the POSP AOD product for different regions across the world, we calculated the R, RMSE, Bias, %EE, and %GCOS between POSP AOD and the corresponding AERONET AOD, as shown in Fig.5 (the global map for MODIS DB/DT are presented in Figs. S4-S5). At most sites, the accuracy of the POSP AOD is high. As indicated in Table 2, 24%, 50%, and 78% of the sites have RMSE less than 0.05, 0.07, and 0.1, respectively. Additionally, 22%, 57%, and 86% of the sites have GCOS fractions greater than 60%, 45%, and 30%, respectively. We observed that R in North America and Europe are slightly lower compared to other regions. This is mainly because the AOD in these regions is relatively low, and the lower spatial resolution of POSP results may be affected by fragmented clouds, leading to overestimation and hence lower R. This argument is substantiated by Fig.5 (B), (C), and (D). Fig.5 (B) shows that RMSE in North America and Europe is closer to zero compared to other regions. And Fig.5 (D) also indicates that the GCOS fraction in these regions is much higher than in other parts of the world. These metrics show a good performance over such regions. We preliminarily infer that a few high-error results influence the R. Additionally, Fig.5 (A) shows that sites in North America and Europe with lower R overlap with sites with positive bias in Fig.5 (C), indirectly confirming that the main reason for lower R in these regions is the influence of overestimated values. It is challenging to completely eliminate the impact of fragmented clouds within pixels solely based on POSP measurement, making slight overestimation at low AOD.

On the other hand, POSP AOD shows high consistency with AERONET AOD in heavily polluted regions such as northern India, central and western Africa, and central South America, although the GCOS fraction is lower. This is because, as AOD

https://doi.org/10.5194/egusphere-2025-91
Preprint. Discussion started: 17 February 2025

increases, the influence of the surface on retrieval accuracy decreases, while the influence of the aerosol model increases. Thus, using a fixed aerosol model inevitably affects the accuracy of retrievals (Levy et al., 2013). This is one of the inherent challenges of intensity retrieval with single-angle observations, and we will gradually address this issue in future algorithm improvements.

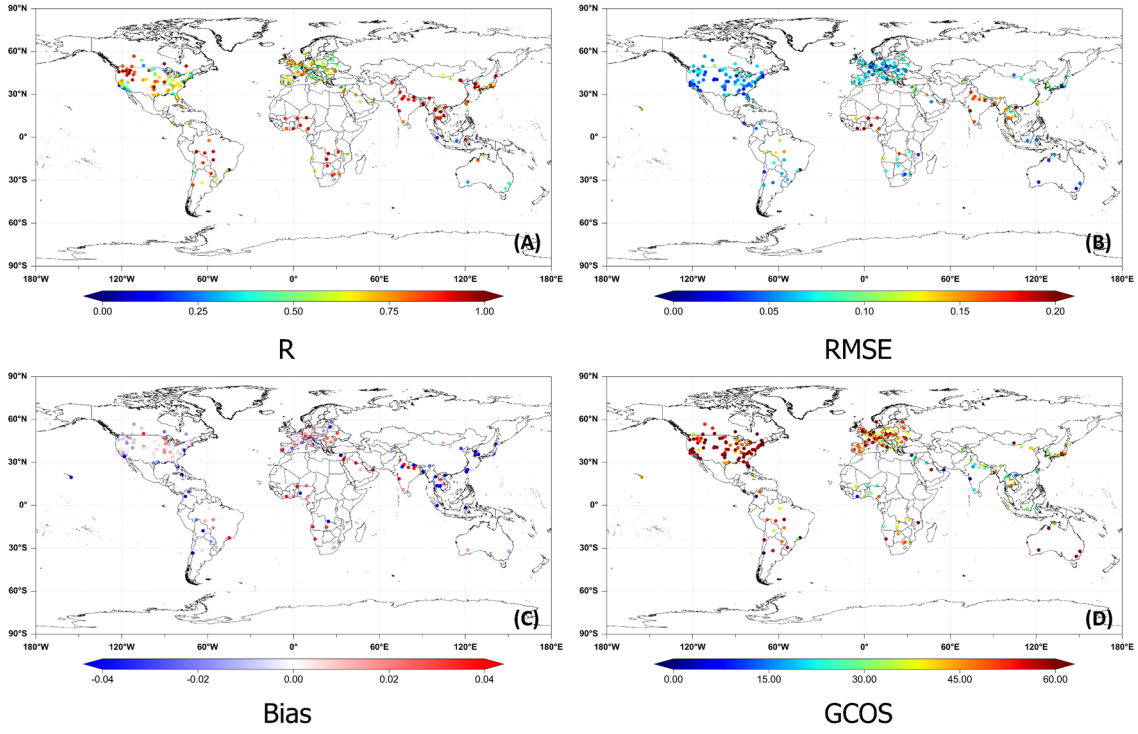

Figure 5: Distribution of site-specific metrics for the comparison of POSP AOD versus AERONET AOD: (A) R, (B) RMSE, (C) Bias, and (D) GCOS.

Table 2: Statistics of POSP AOD.

R	**> 0.7**	**> 0.6**	**> 0.5**
	123 (45%)	173 (64%)	216 (79%)
RMSE	**< 0.05**	**< 0.07**	**< 0.1**
	65 (24%)	137(50%)	213 (78%)
|Bias|	**< 0.04**	**< 0.02**	**< 0.01**
	226(83%)	182(77%)	109(40%)
GCOS	**>60%**	**>45%**	**>30%**
	61(22%)	154(57%)	266(86%)

https://doi.org/10.5194/egusphere-2025-91
Preprint. Discussion started: 17 February 2025

5 Discussion

5.1 Error Analysis

5.1.1 Error analysis of POSP AOD in different seasons

To further assess the impact of different factors on the accuracy of POSP AOD retrievals, we compared AOD bias variations with AE, scattering angle, and NDVI. Fig,6 shows that AE has the least effect on bias, indicating that the algorithm performs well regardless of the particle sizes. However, the uncertainty in the bias decreases as NDVI increases. This trend is not influenced by seasonal changes, indicating that the POSP AOD algorithm tends to produce more accurate results over densely vegetated areas. The accuracy of POSP AOD over different surface types will be discussed in the next section. The DB exhibits anomalies in retrieval accuracy at larger scattering angles (Sayer et al., 2013), and POSP shows a similar pattern. Although the DJF validation results indicate that POSP AOD has the least uncertainty in the range of 170° to 180°, the uncertainty of POSP AOD increases with increasing scattering angle.

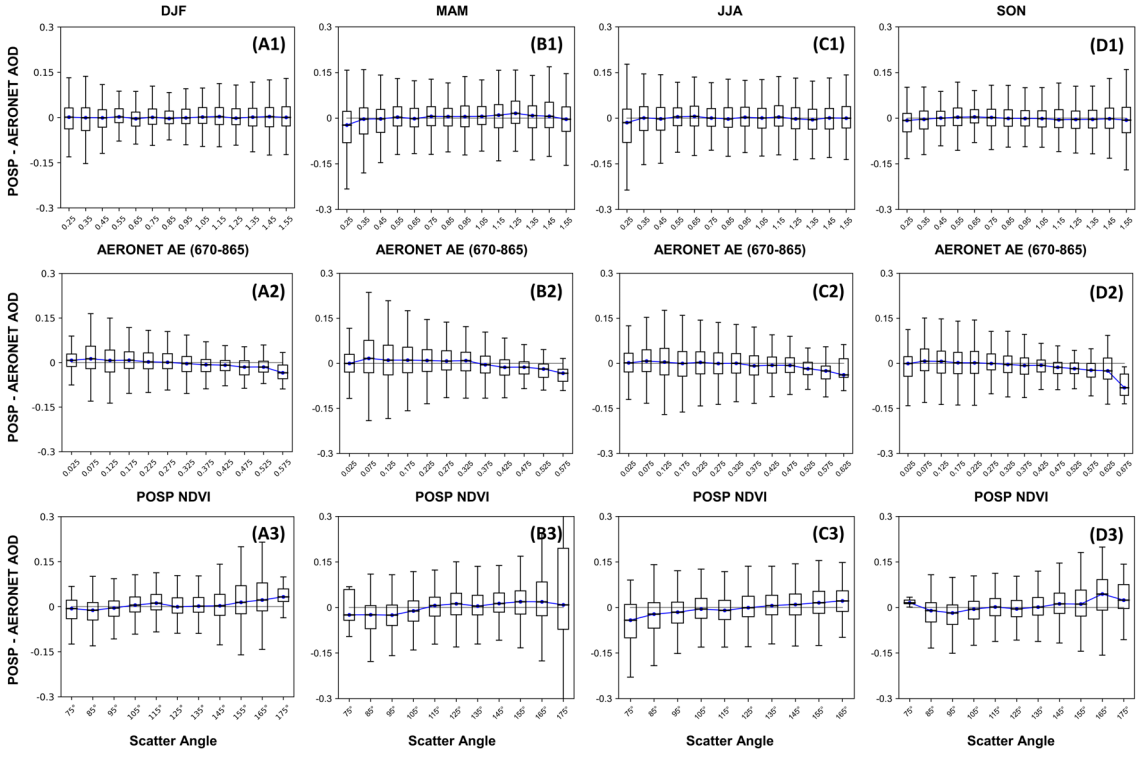

Figure 6: AOD bias as function of (1) AERONET 440–870 nm AE, (2) POSP NDVI, (3) scattering angle, in (A) DJF, (B) MAM, (C) JJA, and (D) SON. The black dots and error bars represent the median, 25th percentiles, and 75th percentiles of the AOD bias.

5.1.2 Error analysis of POSP AOD in different surface types

Fig.7 shows results similar to Fig.6, but for the bias over different land cover types. It is noteworthy that the uncertainty of the AOD over City LC type increases with the scattering angle and increasingly overestimates with increasing scattering angles

https://doi.org/10.5194/egusphere-2025-91
Preprint. Discussion started: 17 February 2025

larger than 135°. The city has complex surface conditions and varied pollution components (Bilal et al., 2022; Wong et al., 2011), and the actual aerosol model might significantly differ from the assumed aerosol model. This indicates that the error sources for retrievals over city are diverse, making it difficult to provide a definitive result on a global scale. We will continue to analyze and improve the retrieval accuracy for city in future research.

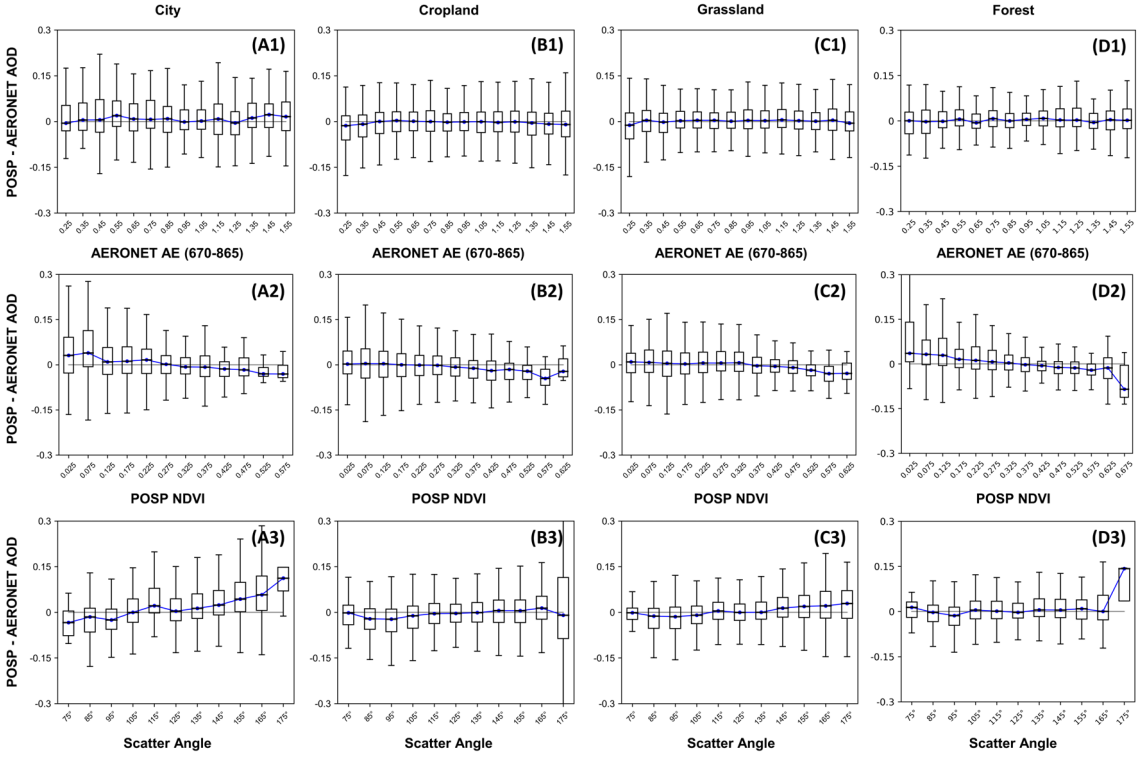

Figure 7: Same as Fig.6 but for different land cover types: (A) city, (B) Cropland, (C) grassland, and (D) forest.

5.2 Comparison of POSP and MODIS AOD

5.2.1 Overall validation

Fig.8 shows comparisons of the POSP and MODIS/Terra AOD for collocated overpasses (with same matching criteria) versus AERONET data, where MODIS AOD was split in DB (11,010 match-ups) and DT (9,211 matchups). The numbers of DB and DT match-ups are different because DT does not provide retrievals over bright surfaces (The validation for DB/DT are presented in Figs. S2-S3, respectively).

The comparison of the POSP and MODIS DB AOD shows that the POSP AOD has a higher accuracy than the MODIS DB AOD, with the fractions within EE of 82.5% and 77.3%, the fraction within GCOS of 52.8% and 47.0% for POSP and DB respectively. The comparison of the POSP and MODIS DT AOD also shows that POSP has higher accuracy, with the fractions within EE of 80.7% and 73.9% for POSP and MODIS, respectively, and the fractions within GCOS of 50.2% and 43.05. Compared to DB, POSP has a higher accuracy than DT. On the other hand, the probability distribution functions in Fig. 8 (C)

https://doi.org/10.5194/egusphere-2025-91
Preprint. Discussion started: 17 February 2025

and (D) show that POSP and DB are nearly unbiased, while DT slightly overestimates AOD. The data in Fig.8 and their statistical metrics show that, within the regions and time frames involved in this cross-validation exercise, the accuracy of POSP AOD is better than that of MODIS AOD for both DB and DT.

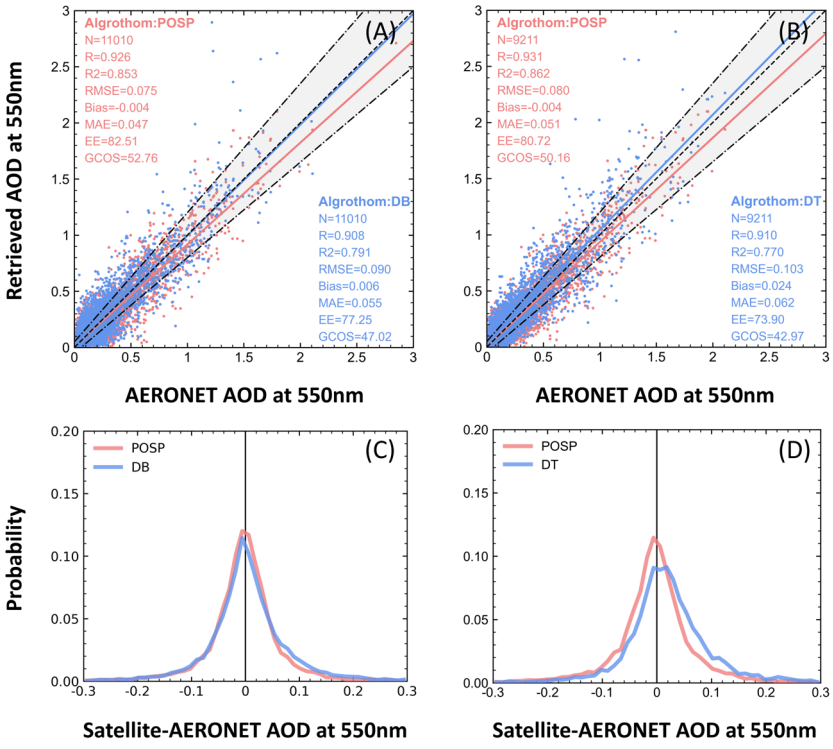

Figure 8: Scatter plots of satellite AOD versus AERONET reference data, where POSP AOD is plotted in red and MODIS AOD in blue, for the DB algorithm (A) and the DT algorithm (B) separately. Probability distribution functions of the differences between satellite AOD (POSP in red and MODIS in blue) and AERONET AOD, for MODIS DB (C) and MODIS DT (D).

5.2.2 Validation over different surface types

The comparison of POSP and MODIS/Terra AOD over four different land cover types (city, cropland, grassland, and forest), using AERONET data as reference, is presented in Fig.9 for DB and in Fig.10 for DT. The data in Fig.9 show the better performance of POSP than that for DB over Cropland, Grassland, and City. However, over Forest, POSP AOD does not show a better performance. Specifically, in terms of R^2, RMSE, and Bias, POSP was better than DB, but other accuracy metrics for POSP were less good than for DB. Considering the small differences in these accuracy metrics, we conclude that the accuracy of POSP and DB for Forest is similar.

Fig.10 shows that the performance of POSP over Cropland, Grassland, and City is better than that of DT, but the accuracy of POSP and DT for Forest is similar. It is noteworthy that from the comparison of bias histograms for different land cover types, the POSP AOD is nearly unbiased in all scenarios, whereas DB shows a positive bias in City, and DT shows a positive bias in City, Cropland, and Forest.

https://doi.org/10.5194/egusphere-2025-91
Preprint. Discussion started: 17 February 2025

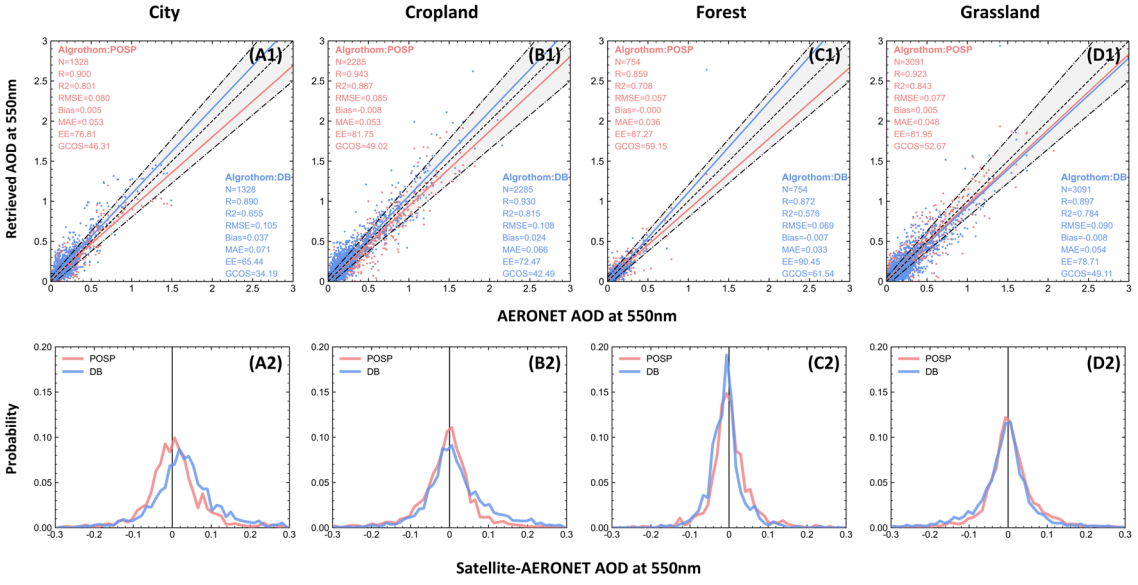

Figure 9: As Fig. 8, for AOD from POSP and MODIS/TERRA DB, over different land cover types: (A) city, (B) Cropland, (C) grassland, and (D) forest.

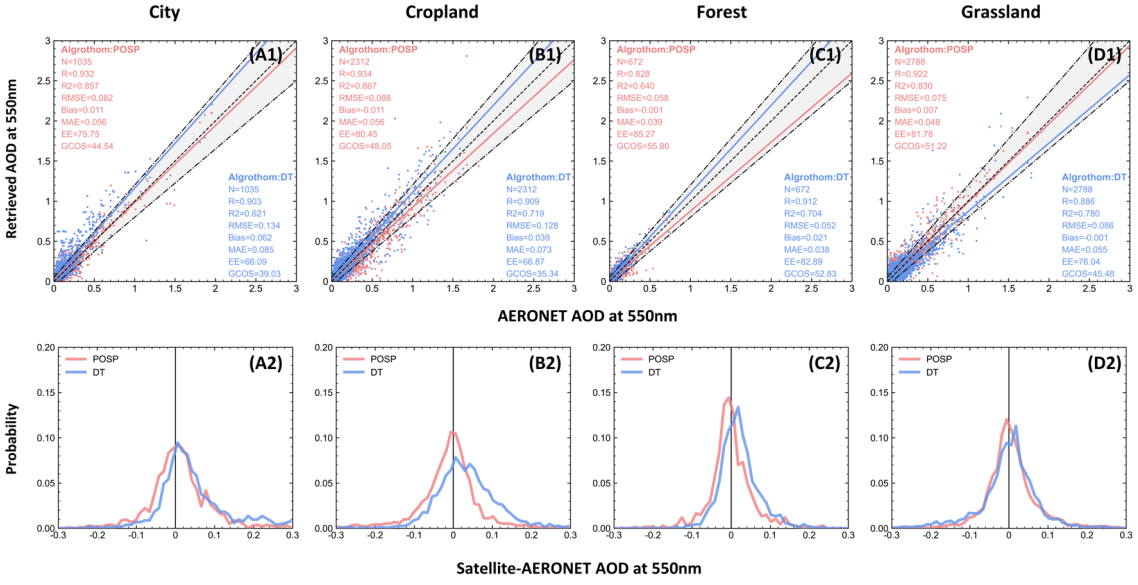

Figure 10: As Fig.9, but for DT.

5.2.3 Comparison of the spatial distributions of AOD from POSP and MODIS/Terra

Fig.11 shows the spatial distributions of seasonally averaged POSP AOD, and the difference between the seasonally averaged POSP and MODIS/Terra AOD are presented in Figs. S8-S9 (the spatial distributions of seasonally averaged POSP AOD are presented in Figs. S6-S7). During DJF, AOD could not be retrieved over high-latitude regions due to the presence of snow and ice.

https://doi.org/10.5194/egusphere-2025-91
Preprint. Discussion started: 17 February 2025

Overall, AOD was higher during MMA and JJA than during DJF and SON in 2022. These quarterly characteristics align with those of other satellite products (Chen et al., 2020; Fan et al., 2023). Global seasonal mean AOD variations are primarily influenced by changes in climatic conditions and anthropogenic impacts. For instance, coarse-dominated AOD tend to be higher in regions like northern Africa or the Middle East during active dust and sand events (Farahat, 2019). Frequent biomass burning events contribute to elevated AOD in south-central Africa (Tummon et al., 2010). Furthermore, high AOD persists in eastern China and northern India due to active industrial production and biomass burning events (de Leeuw et al., 2018; Gupta et al., 2021). Conversely, during winter in the Northern Hemisphere the AOD is lower due to stable atmospheric conditions and reduced atmospheric vertical convective activity (Liu et al., 2022; Zhao et al., 2018).

Regarding the regional distribution of AOD, the high AOD regions identified by the POSP AOD algorithm include northern India, south-central Africa, and central South America, aligning with the spatial distribution of MODIS products. Moreover, compared to MODIS DB (in Fig. S8), the spatial differences between POSP AOD and MODIS DT (in Fig. S9) are smaller. This may be because DT lacks retrieval results over desert areas, while the underestimation of POSP AOD in these regions leads to discrepancies between POSP AOD and DB AOD. In general, the results indicate a high degree of agreement between POSP and MODIS AOD, with differences predominantly falling within the (-0.2, 0.2) range. Therefore, despite differences in algorithm principles, spatial resolution, and other processing procedures between POSP and MODIS products, POSP demonstrates relatively high consistency with MODIS products across most regions globally.

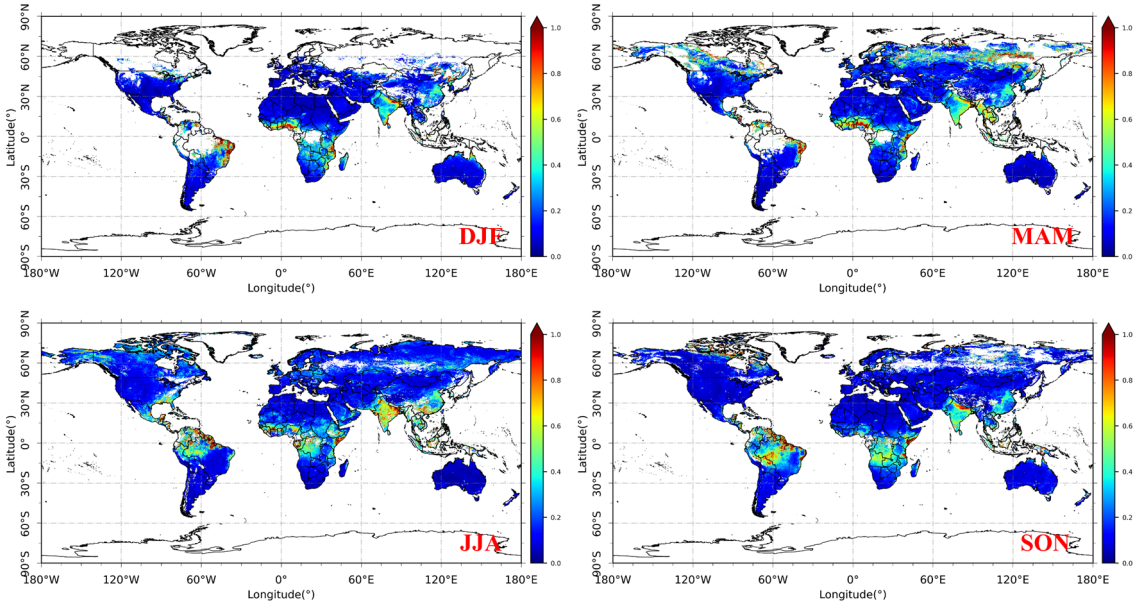

Figure 11: Maps of the seasonally averaged AOD derived from POSP, for the winter (DJF: December–January–February), spring (MAM: March–April-May,) summer (JJA: June–July–August), and autumn (SON: September–October–November).

https://doi.org/10.5194/egusphere-2025-91
Preprint. Discussion started: 17 February 2025

5.3 Time-series analysis of priority regions

POSP is capable of achieving global coverage within 1–2 days for its wide swath (~1850 km), providing a comprehensive monitoring capability for atmospheric conditions worldwide. In this study, we performed a time series analysis focusing on representative polluted regions. The North China Plain (NCP) is a key region for aerosol research due to its unique economic and geographical characteristics, as discussed in previous study (Deng et al., 2011; Li et al., 2017a; Liu et al., 2011). The station Beijing_CAMS is located within Beijing. As shown in Fig.12 (A), POSP consistently exhibited the lowest RMSE across all stations, with retrieval counts equal to or greater than those of MODIS DB. Notably, severe pollution events (AOD > 1.5) were recorded in the Beijing area at the end of April, and August. While POSP AOD tends to slightly underestimate AOD compared to the overestimated MODIS DB AOD, it shows a higher overall consistency with AERONET AOD for the 2022. As South Korea's primary economic hub, Seoul is a highly urbanized area where air pollution has been a significant environmental concern. Located downwind in East Asia, Seoul is a crucial region for studying aerosols and their transport processes (Kim et al., 2007; Oh et al., 2015). The major sources of air pollution include traffic emissions and increased $PM_{2.5}$ due to winter heating demands (Kim et al., 2022). Additionally, regional transport significantly influences Seoul's air quality (Kim et al., 2016). During the autumn and winter, temperature inversions frequently occur, trapping pollutants near the surface and exacerbating pollution levels (Seo et al., 2018). As shown in Fig.12 (B), Seoul National University (Seoul_SNU) is located within the Seoul metropolitan area. In the 2022, severe pollution events mainly occurred in late April, May, November, and December, which does not coincide with the severe pollution periods in Beijing shown in Fig.12 (A). This discrepancy suggests that long-range transport from Beijing to Seoul was unlikely to be the cause. Instead, based on Seoul's local historical observations, it is likely that these pollution events were primarily due to locally emitted fine particulate matter (Kim et al., 2020). Similar to the findings for the Beijing area, POSP showed the lowest RMSE at Seoul station, with retrieval counts equal to or greater than those of MODIS DB.

India is one of the most severely air-polluted countries in the world, especially in the northern Indian plains (Vellalassery et al., 2021). This region's aerosol composition is highly complex, consisting of both natural sources, such as biomass burning that releases significant amounts of organic carbon and black carbon, and anthropogenic sources, including industrial and vehicular emissions that contribute sulfates, nitrates, black carbon, and organic aerosols (David et al., 2018; Ghude et al., 2016). Thus, northern India is a critical region for aerosol studies. As illustrated in Fig.12 (C) and (D), Amity University, and Gandhi College are all located in the western part of northern India. In the 2022, severe pollution events primarily occurred at the end of April and in May, with Gandhi College station lacking observations between June and September. Across all stations, POSP consistently showed the lowest RMSE, indicating superior retrieval accuracy. Notably, at Gandhi College, the RMSE of POSP AOD (0.21) was significantly lower than that of MODIS DB AOD (0.29), highlighting the enhanced precision of POSP in this region.

https://doi.org/10.5194/egusphere-2025-91
Preprint. Discussion started: 17 February 2025

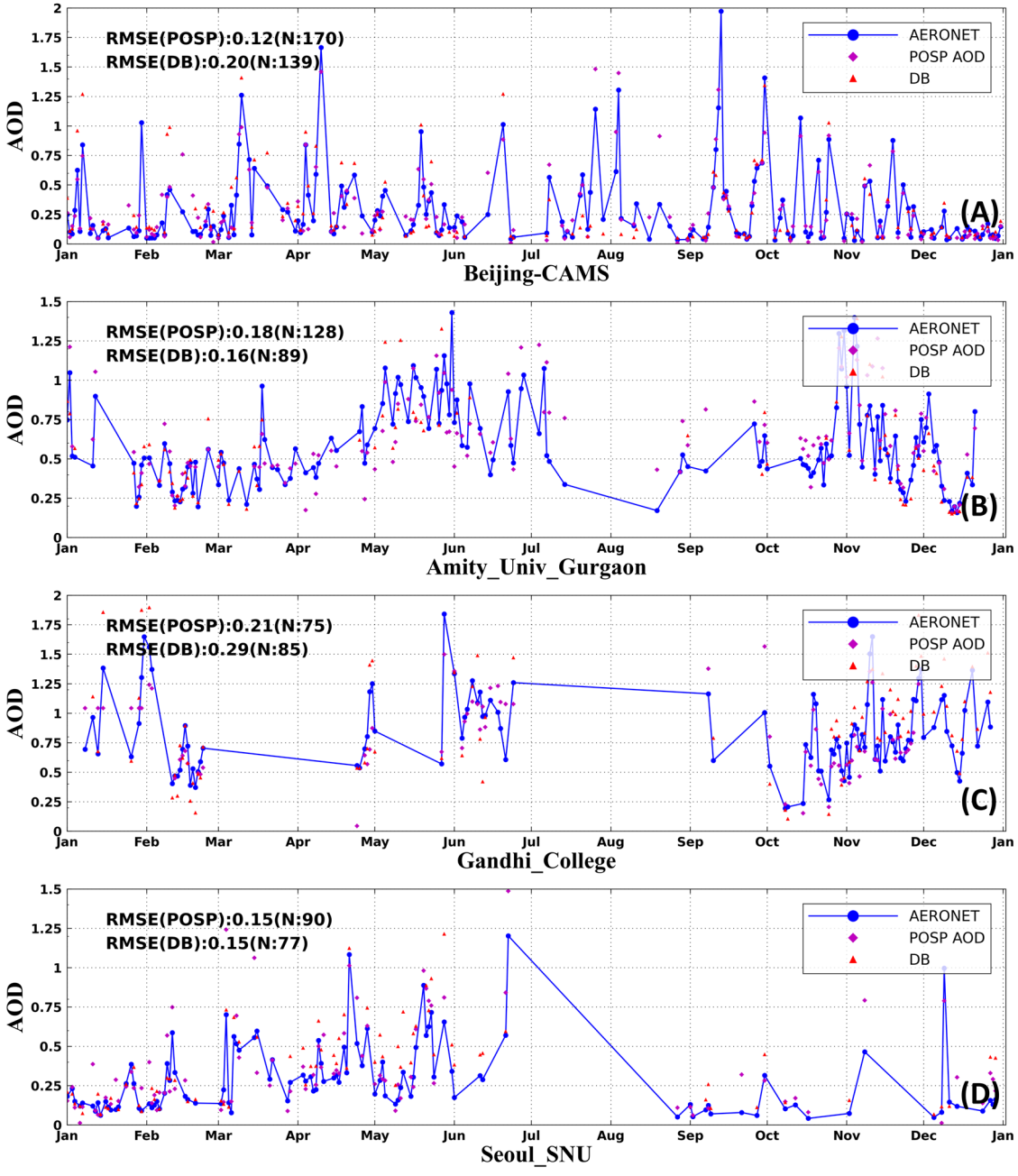

Figure 12: Time series of the POSP AOD (purple diamond) and DB AOD (red triangle) against AERONET (blue circle) measurements over the (A) Beijing-CAMS, (B) Amity University, (C) Gandhi College, and (D) Seoul University.

https://doi.org/10.5194/egusphere-2025-91
Preprint. Discussion started: 17 February 2025

6 Discussion

This study focuses on the detailed performance of the newly proceed POSP AOD product. To this end, data from 276 global AERONET sites and MODIS/Terra AOD products were collected. The POSP AOD was evaluated and analyzed in two ways: 1) direct validation versus AERONET observations at seasonal, regional, and site-specific scales; 2) cross-validation of POSP AOD and MODIS aerosol products from both he DB and DT algorithms, land cover types, and spatial distribution differences. The principal findings are as follows:

1. The validation of POSP AOD with AERONET AOD shows the good performance of the POSP algorithm with validation metrics reported in Section 4.1. The fraction within the expected error is 78.45% and fraction within the GCOS is 48.6%. The accuracy of the POSP AOD varies significantly across different seasons, with the highest accuracy in the DJF (R^2 of 0.854, RMSE of 0.080) and the lowest in the JJA (R^2 of 0.667, RMSE of 0.083). We also compared the accuracy of POSP AOD over different land cover types, finding that high-accuracy results are mainly concentrated in areas with high vegetation coverage, with croplands achieving the highest accuracy (R^2 of 0.859, RMSE of 0.093). However, the accuracy decreases over bright surface areas such as urban and dessert. Further error analysis shows that the accuracy of POSP AOD is mainly influenced by surface vegetation cover and observation geometry. As NDVI or scattering angle increases, the uncertainty of POSP AOD decreases. Nonetheless, regardless of these conditions, POSP AOD consistently provides results with low bias.
2. Global site-scale validation results show that POSP AOD is more consistent with AERONET AOD in high AOD regions than in low AOD regions. In contrast, the fraction of POSP AOD within the GCOS requirements is higher in high AOD regions than in low AOD regions. When comparing RMSE, we found that POSP AOD shows lower values in low AOD regions such as North America and Europe, while it exhibits higher values in high AOD regions such as northern India and central-western Africa. Additionally, POSP AOD tends to underestimate AOD in Asia and overestimate AOD in Europe. Thus, it is challenging to determine the global accuracy distribution of POSP AOD based solely on a single parameter. However, using the fraction within GCOS as the sole metric, 57% of the sites have GCOS > 45%, and 78% of the sites show lower uncertainty in POSP AOD retrieval (RMSE < 0.1).

Comparative analysis with MODIS AOD products shows similar spatial distributions of POSP and MODIS AOD. Moreover, in cross-validation, the performance of the POSP AOD is better than that of the MODIS AOD. For DB, the comparison metrics are as follows: R^2 of 0.853/0.791 for POSP/MODIS, RMSE of 0.075/0.090, Bias of -0.004/0.006, fraction within EE of 82.51%/77.25%, fraction within GCOS of 52.76%/47.02% (POSP/DB); and for DT: R of 0.931/0.910, R^2 of 0.862/0.770, RMSE of 0.080/0.103, Bias of -0.004/0.024, fraction within EE of 80.72%/73.90%, the fraction within GCOS of 50.16%/42.97% (POSP/DT). Comparison over different surface types shows that POSP AOD is more accurate than DB over City, Cropland, and Grassland areas, and better than DT under all surface types.

https://doi.org/10.5194/egusphere-2025-91
Preprint. Discussion started: 17 February 2025

Data availability

The POSP/Gaofen-5(02) level-1 data can be downloaded from the website https://data.cresda.cn/ (last access: 1 January 2025). The AERONET data can be downloaded from the website https://aeronet.gsfc.nasa.gov/ (last access: 1 January 2025). The MODIS/Terra aerosol data can be accessed through the website https://ladsweb.modaps.eosdis.nasa.gov/ (last access: 1 January 2025).

Auth contributions.

Z.J. conducted the data analysis. Z.L. provided data. Z.J. designed the program code. Z.J. wrote this manuscript. Z.Z., Y.M., Z.S., C.F., and Q.Y. reviewed this manuscript. All authors have read and agreed to the published version of the manuscript.

Competing interests.

The authors declare that they have no conflict of interest.

Financial support.

This work was supported by the National Natural Science Foundation of China (grant nos.41925019, 42305151), and the National Key R&D Program of China (2023YFB3907405). The participation of Gerrit de Leeuw was supported by the Chinese Academy of Sciences President's International Fellowship Initiative (PIFI) (grant nos. 2025PVA0014).

References

Ångström, A.: On the Atmospheric Transmission of Sun Radiation and on Dust in the Air, Geogr. Ann., 11, 156–166, https://doi.org/10.1080/20014422.1929.11880498, 1929.

Bai, K., Li, K., Wu, C., Chang, N.-B., and Guo, J.: A homogenized daily in situ PM 2.5 concentration dataset from the national air quality monitoring network in China, Earth Syst. Sci. Data, 12, 3067–3080, 2020.

Beig, G., Sahu, S., Anand, V., Bano, S., Maji, S., Rathod, A., Korhale, N., Sobhana, S. B., Parkhi, N., Mangaraj, P., and others: India's Maiden air quality forecasting framework for megacities of divergent environments: The SAFAR-project, Environ. Model. Softw., 145, 105204, 2021.

Bellouin, N., Quaas, J., Gryspeerdt, E., Kinne, S., Stier, P., Watson-Parris, D., Boucher, O., Carslaw, K. S., Christensen, M., Daniau, A.-L., and others: Bounding global aerosol radiative forcing of climate change, Rev. Geophys., 58, e2019RG000660, 2020.

https://doi.org/10.5194/egusphere-2025-91
Preprint. Discussion started: 17 February 2025

Bergametti, G., Dutot, A.-L., Buat-Menard, P., Losno, R., and Remoudaki, E.: Seasonal variability of the elemental composition of atmospheric aerosol particles over the northwestern Mediterranean, Tellus B Chem. Phys. Meteorol., 41, 353–361, 1989.

Bilal, M., Mhawish, A., Ali, M. A., Nichol, J. E., Leeuw, G. de, Khedher, K. M., Mazhar, U., Qiu, Z., Bleiweiss, M. P., and Nazeer, M.: Integration of surface reflectance and aerosol retrieval algorithms for multi-resolution aerosol optical depth retrievals over urban areas, Remote Sens., 14, 373, 2022.

Che, H., Zhang, X.-Y., Xia, X., Goloub, P., Holben, B., Zhao, H., Wang, Y., Zhang, X.-C., Wang, H., and Blarel, L.: Ground-based aerosol climatology of China: aerosol optical depths from the China Aerosol Remote Sensing Network (CARSNET) 2002–2013, Atmospheric Chem. Phys., 15, 7619–7652, 2015.

Che, Y., Xue, Y., Mei, L., Guang, J., She, L., Guo, J., Hu, Y., Xu, H., He, X., Di, A., and Fan, C.: Technical note: Intercomparison of three AATSR Level 2 (L2) AOD products overChina, Atmospheric Chem. Phys., 16, 9655–9674, https://doi.org/10.5194/acp-16-9655-2016, 2016.

Chen, C., Dubovik, O., Fuertes, D., Litvinov, P., Lapyonok, T., Lopatin, A., Ducos, F., Derimian, Y., Herman, M., Tanré, D., Remer, L. A., Lyapustin, A., Sayer, A. M., Levy, R. C., Hsu, N. C., Descloitres, J., Li, L., Torres, B., Karol, Y., Herrera, M., Herreras, M., Aspetsberger, M., Wanzenboeck, M., Bindreiter, L., Marth, D., Hangler, A., and Federspiel, C.: Validation of GRASP algorithm product from POLDER/PARASOL dataand assessment of multi-angular polarimetry potential for aerosolmonitoring, Atmosphere – Atmospheric Chemistry and Physics, https://doi.org/10.5194/essd-2020-224, 2020.

Chen, C., Dubovik, O., Schuster, G. L., Chin, M., Henze, D. K., Lapyonok, T., Li, Z., Derimian, Y., and Zhang, Y.: Multi-angular polarimetric remote sensing to pinpoint global aerosol absorption and direct radiative forcing, Nat. Commun., 13, 7459, https://doi.org/10.1038/s41467-022-35147-y, 2022.

Chu, D. A., Kaufman, Y. J., Ichoku, C., Remer, L. A., Tanré, D., and Holben, B. N.: Validation of MODIS aerosol optical depth retrieval over land, Geophys. Res. Lett., 29, https://doi.org/10.1029/2001GL013205, 2002.

Cobourn, W. G.: Accuracy and reliability of an automated air quality forecast system for ozone in seven Kentucky metropolitan areas, Atmos. Environ., 41, 5863–5875, 2007.

David, L. M., Ravishankara, A., Kodros, J. K., Venkataraman, C., Sadavarte, P., Pierce, J. R., Chaliyakunnel, S., and Millet, D. B.: Aerosol optical depth over India, J. Geophys. Res. Atmospheres, 123, 3688–3703, 2018.

De Leeuw, G., Sogacheva, L., Rodriguez, E., Kourtidis, K., Georgoulias, A. K., Alexandri, G., Amiridis, V., Proestakis, E., Marinou, E., Xue, Y., and Van Der A, R.: Two decades of satellite observations of AOD over mainland China using ATSR-2, AATSR and MODIS/Terra: data set evaluation and large-scale patterns, Atmospheric Chem. Phys., 18, 1573–1592, https://doi.org/10.5194/acp-18-1573-2018, 2018.

Deng, Z., Zhao, C., Ma, N., Liu, P., Ran, L., Xu, W., Chen, J., Liang, Z., Liang, S., Huang, M., and others: Size-resolved and bulk activation properties of aerosols in the North China Plain, Atmospheric Chem. Phys., 11, 3835–3846, 2011.

https://doi.org/10.5194/egusphere-2025-91
Preprint. Discussion started: 17 February 2025

Dubovik, O., Holben, B., Eck, T. F., Smirnov, A., Kaufman, Y. J., King, M. D., Tanré, D., and Slutsker, I.: Variability of Absorption and Optical Properties of Key Aerosol Types Observed in Worldwide Locations, J. Atmospheric Sci., 59, 590–608, https://doi.org/10.1175/1520-0469(2002)059<0590:VOAAOP>2.0.CO;2, 2002.

Eck, T. F., Holben, B., Reid, J., Dubovik, O., Smirnov, A., O'neill, N., Slutsker, I., and Kinne, S.: Wavelength dependence of the optical depth of biomass burning, urban, and desert dust aerosols, J. Geophys. Res. Atmospheres, 104, 31333–31349, 1999.

Fan, R., Ma, Y., Jin, S., Gong, W., Liu, B., Wang, W., Li, H., and Zhang, Y.: Validation, analysis, and comparison of MISR V23 aerosol optical depth products with MODIS and AERONET observations, Sci. Total Environ., 856, 159117, https://doi.org/10.1016/j.scitotenv.2022.159117, 2023.

Farahat, A.: Comparative analysis of MODIS, MISR, and AERONET climatology over the Middle East and North Africa, in: Annales Geophysicae, 49–64, 2019.

Ghude, S. D., Chate, D., Jena, C., Beig, G., Kumar, R., Barth, M., Pfister, G., Fadnavis, S., and Pithani, P.: Premature mortality in India due to PM2. 5 and ozone exposure, Geophys. Res. Lett., 43, 4650–4658, 2016.

Giles, D. M., Sinyuk, A., Sorokin, M. G., Schafer, J. S., Smirnov, A., Slutsker, I., Eck, T. F., Holben, B. N., Lewis, J. R., Campbell, J. R., and others: Advancements in the Aerosol Robotic Network (AERONET) Version 3 database–automated near-real-time quality control algorithm with improved cloud screening for Sun photometer aerosol optical depth (AOD) measurements, Atmospheric Meas. Tech., 12, 169–209, 2019.

Ginoux, P., Chin, M., Tegen, I., Prospero, J. M., Holben, B., Dubovik, O., and Lin, S.-J.: Sources and distributions of dust aerosols simulated with the GOCART model, J. Geophys. Res. Atmospheres, 106, 20255–20273, 2001.

Goloub, P., Li, Z., Dubovik, O., Blarel, L., Podvin, T., Jankowiak, I., Lecoq, R., Deroo, C., Chatenet, B., Morel, J.-P., and others: PHOTONS/AERONET sunphotometer network overview: description, activities, results, in: Fourteenth International Symposium on Atmospheric and Ocean Optics/Atmospheric Physics, 218–232, 2008.

Guo, J., Deng, M., Lee, S. S., Wang, F., Li, Z., Zhai, P., Liu, H., Lv, W., Yao, W., and Li, X.: Delaying precipitation and lightning by air pollution over the Pearl River Delta. Part I: Observational analyses, J. Geophys. Res. Atmospheres, 121, 6472–6488, https://doi.org/10.1002/2015JD023257, 2016.

Gupta, A., Kant, Y., Mitra, D., and Chauhan, P.: Spatio-temporal distribution of INSAT-3D AOD derived particulate matter concentration over India, Atmospheric Pollut. Res., 12, 159–172, 2021.

He, Q. and Huang, B.: Satellite-based mapping of daily high-resolution ground PM2. 5 in China via space-time regression modeling, Remote Sens. Environ., 206, 72–83, 2018.

He, Q., Zhang, M., and Huang, B.: Spatio-temporal variation and impact factors analysis of satellite-based aerosol optical depth over China from 2002 to 2015, Atmos. Environ., 129, 79–90, https://doi.org/10.1016/j.atmosenv.2016.01.002, 2016.

Hoff, R. M., Engel-Cox, J. A., Dimmick, F., Szykman, J. J., Johns, B., Kondragunta, S., Rogers, R., McCann, K., Chu, D. A., Torres, O., and others: 3D-AQS: a three-dimensional air quality system, in: Remote Sensing of Aerosol and Chemical Gases, Model Simulation/Assimilation, and Applications to Air Quality, 629901, 2006.

https://doi.org/10.5194/egusphere-2025-91
Preprint. Discussion started: 17 February 2025

Holben, B. N., Eck, T. F., Slutsker, I. al, Tanré, D., Buis, J. P., Setzer, A., Vermote, E., Reagan, J. A., Kaufman, Y. J., and Nakajima, T.: AERONET—A federated instrument network and data archive for aerosol characterization, Remote Sens. Environ., 66, 1–16, 1998.

Hou, W., Li, Z., Wang, J., Xu, X., Goloub, P., and Qie, L.: Improving Remote Sensing of Aerosol Microphysical Properties by Near-Infrared Polarimetric Measurements Over Vegetated Land: Information Content Analysis, J. Geophys. Res. Atmospheres, 123, 2215–2243, 2018.

Hsu, N., Jeong, M.-J., Bettenhausen, C., Sayer, A., Hansell, R., Seftor, C., Huang, J., and Tsay, S.-C.: Enhanced Deep Blue aerosol retrieval algorithm: The second generation, J. Geophys. Res. Atmospheres, 118, 9296–9315, 2013.

Ichoku, C., Chu, D. A., Mattoo, S., Kaufman, Y. J., Remer, L. A., Tanré, D., Slutsker, I., and Holben, B. N.: A spatio-temporal approach for global validation and analysis of MODIS aerosol products, Geophys. Res. Lett., 29, MOD1-1, 2002.

Ji, Z., Ma, Y., de Leeuw, G., Shi, Z., and Li, Z.: An Enhanced Aerosol Optical Depth Retrieval Algorithm for Particulate Observing Scanning Polarimeter (POSP) Data Over Land, IEEE Trans. Geosci. Remote Sens., 63, 1–18, https://doi.org/10.1109/TGRS.2024.3514170, 2025.

Kaufman, Y. J., Tanré, D., Remer, L. A., Vermote, E. F., Chu, A., and Holben, B. N.: Operational remote sensing of tropospheric aerosol over land from EOS moderate resolution imaging spectroradiometer, J. Geophys. Res. Atmospheres, 102, 17051–17067, https://doi.org/10.1029/96JD03988, 1997.

Kim, H.-S., Huh, J.-B., Hopke, P. K., Holsen, T. M., and Yi, S.-M.: Characteristics of the major chemical constituents of PM2. 5 and smog events in Seoul, Korea in 2003 and 2004, Atmos. Environ., 41, 6762–6770, 2007.

Kim, H.-S., Chung, Y.-S., and Yoon, M.-B.: An analysis on the impact of large-scale transports of dust pollution on air quality in East Asia as observed in central Korea in 2014, Air Qual. Atmosphere Health, 9, 83–93, 2016.

Kim, Y., Yi, S.-M., and Heo, J.: Fifteen-year trends in carbon species and PM2. 5 in Seoul, South Korea (2003–2017), Chemosphere, 261, 127750, 2020.

Kim, Y., Jeon, K., Park, J., Shim, K., Kim, S.-W., Shin, H.-J., Yi, S.-M., and Hopke, P. K.: Local and transboundary impacts of PM2. 5 sources identified in Seoul during the early stage of the COVID-19 outbreak, Atmospheric Pollut. Res., 13, 101510, 2022.

Lee, H., Calvin, K., Dasgupta, D., Krinner, G., Mukherji, A., Thorne, P., Trisos, C., Romero, J., Aldunce, P., Barret, K., and others: IPCC, 2023: Climate Change 2023: Synthesis Report, Summary for Policymakers. Contribution of Working Groups I, II and III to the Sixth Assessment Report of the Intergovernmental Panel on Climate Change [Core Writing Team, H. Lee and J. Romero (eds.)]. IPCC, Geneva, Switzerland., 2023.

de Leeuw, G., Kinne, S., Léon, J.-F., Pelon, J., Rosenfeld, D., Schaap, M., Veefkind, P. J., Veihelmann, B., Winker, D. M., and von Hoyningen-Huene, W.: Retrieval of aerosol properties, Remote Sens. Tropospheric Compos. Space, 259–313, 2011.

Lei, X., Liu, Z., Tao, F., Dong, H., Hou, W., Xiang, G., Qie, L., Meng, B., Li, C., and Chen, F.: Data Comparison and Cross-Calibration between Level 1 Products of DPC and POSP Onboard the Chinese GaoFen-5 (02) Satellite, Remote Sens., 15, 1933, 2023.

https://doi.org/10.5194/egusphere-2025-91
Preprint. Discussion started: 17 February 2025

Levy, R. C., Remer, L. A., and Dubovik, O.: Global aerosol optical properties and application to Moderate Resolution Imaging Spectroradiometer aerosol retrieval over land, J. Geophys. Res. Atmospheres, 112, 2006JD007815, https://doi.org/10.1029/2006JD007815, 2007.

Levy, R. C., Remer, L. A., Kleidman, R. G., Mattoo, S., Ichoku, C., Kahn, R., and Eck, T. F.: Global evaluation of the Collection 5 MODIS dark-target aerosol products over land, Atmospheric Chem. Phys., 10, 10399–10420, https://doi.org/10.5194/acp-10-10399-2010, 2010.

Levy, R. C., Mattoo, S., Munchak, L. A., Remer, L. A., Sayer, A. M., Patadia, F., and Hsu, N. C.: The Collection 6 MODIS aerosol products over land and ocean, Atmospheric Meas. Tech., 6, 2989–3034, https://doi.org/10.5194/amt-6-2989-2013, 2013.

Li, H., Zhang, Q., Zhang, Q., Chen, C., Wang, L., Wei, Z., Zhou, S., Parworth, C., Zheng, B., Canonaco, F., and others: Wintertime aerosol chemistry and haze evolution in an extremely polluted city of the North China Plain: significant contribution from coal and biomass combustion, Atmospheric Chem. Phys., 17, 4751–4768, 2017a.

Li, Z., Guo, J., Ding, A., Liao, H., Liu, J., Sun, Y., Wang, T., Xue, H., Zhang, H., and Zhu, B.: Aerosol and boundary-layer interactions and impact on air quality, Natl. Sci. Rev., 4, 810–833, 2017b.

Li, Z., Hou, W., Hong, J., Zheng, F., Luo, D., Wang, J., Gu, X., and Qiao, Y.: Directional Polarimetric Camera (DPC): Monitoring aerosol spectral optical properties over land from satellite observation, J. Quant. Spectrosc. Radiat. Transf., 218, 21–37, https://doi.org/10.1016/j.jqsrt.2018.07.003, 2018a.

Li, Z., Hou, W., Hong, J., Fan, C., Wei, Y., Liu, Z., Lei, X., Qiao, Y., Hasekamp, O. P., Fu, G., Wang, J., Dubovik, O., Qie, L., Zhang, Y., Xu, H., Xie, Y., Song, M., Zou, P., Luo, D., Wang, Y., and Tu, B.: The polarization crossfire (PCF) sensor suite focusing on satellite remote sensing of fine particulate matter PM2.5 from space, J. Quant. Spectrosc. Radiat. Transf., 286, 108217, https://doi.org/10.1016/j.jqsrt.2022.108217, 2022.

Li, Z. Q., Xu, H., Li, K. T., Li, D. H., Xie, Y. S., Li, L., Zhang, Y., Gu, X. F., Zhao, W., and Tian, Q. J.: Comprehensive study of optical, physical, chemical, and radiative properties of total columnar atmospheric aerosols over China: An overview of Sun–Sky Radiometer Observation Network (SONET) measurements, Bull. Am. Meteorol. Soc., 99, 739–755, 2018b.

Liangfu, C., SHANG, H., Meng, F., Jinhua, T., Letu, H., ZHANG, Y., Hongmei, W., CHENG, L., ZHANG, X., Lesi, W., and others: Mission overview of the GF-5 satellite for atmospheric parameter monitoring, Natl. Remote Sens. Bull., 25, 1917–1931, 2021.

Liu, B., Ma, X., Ma, Y., Li, H., Jin, S., Fan, R., and Gong, W.: The relationship between atmospheric boundary layer and temperature inversion layer and their aerosol capture capabilities, Atmospheric Res., 271, 106121, 2022.

Liu, P., Zhao, C., Göbel, T., Hallbauer, E., Nowak, A., Ran, L., Xu, W., Deng, Z., Ma, N., Mildenberger, K., and others: Hygroscopic properties of aerosol particles at high relative humidity and their diurnal variations in the North China Plain, Atmospheric Chem. Phys., 11, 3479–3494, 2011.

Moreno, S.: The WMO Global Atmosphere Watch Programme new implementation plan and strategic objectives, in: EGU General Assembly Conference Abstracts, EGU-14442, 2023.

https://doi.org/10.5194/egusphere-2025-91
Preprint. Discussion started: 17 February 2025

Myhre, G., Bellouin, N., Berglen, T. F., Berntsen, T. K., Boucher, O., Grini, A., Ivar, S. M., Johnsrud, I., Michael, I. M., Stordal, F., and others: Comparison of the radiative properties and direct radiative effect of aerosols from a global aerosol model and remote sensing data over ocean, Tellus B Chem. Phys. Meteorol., 59, 115–129, 2007.

Oh, H.-R., Ho, C.-H., Kim, J., Chen, D., Lee, S., Choi, Y.-S., Chang, L.-S., and Song, C.-K.: Long-range transport of air pollutants originating in China: A possible major cause of multi-day high-PM10 episodes during cold season in Seoul, Korea, Atmos. Environ., 109, 23–30, 2015.

Popp, T., De Leeuw, G., Bingen, C., Brühl, C., Capelle, V., Chedin, A., Clarisse, L., Dubovik, O., Grainger, R., Griesfeller, J., and others: Development, production and evaluation of aerosol climate data records from European satellite observations (Aerosol_cci), Remote Sens., 8, 421, 2016.

Rabha, S. and Saikia, B. K.: Advanced micro-and nanoscale characterization techniques for carbonaceous aerosols, in: Handbook of Nanomaterials in Analytical Chemistry, Elsevier, 449–472, 2020.

Rosenfeld, D.: Suppression of rain and snow by urban and industrial air pollution, science, 287, 1793–1796, 2000.

Rosenfeld, D., Andreae, M. O., Asmi, A., Chin, M., de Leeuw, G., Donovan, D. P., Kahn, R., Kinne, S., Kivekäs, N., Kulmala, M., and others: Global observations of aerosol-cloud-precipitation-climate interactions, Rev. Geophys., 52, 750–808, 2014.

Sayer, A. M., Hsu, N., Bettenhausen, C., and Jeong, M.-J.: Validation and uncertainty estimates for MODIS Collection 6 “Deep Blue” aerosol data, J. Geophys. Res. Atmospheres, 118, 7864–7872, 2013.

Secretariat, G.: Systematic observation requirements for satellite-based products for climate, GCOS Implement. Plan, 2006.

Seo, J., Park, D.-S. R., Kim, J. Y., Youn, D., Lim, Y. B., and Kim, Y.: Effects of meteorology and emissions on urban air quality: a quantitative statistical approach to long-term records (1999–2016) in Seoul, South Korea, Atmospheric Chem. Phys., 18, 16121–16137, 2018.

Shi, Z., Xie, Y., Li, Z., Zhang, Y., Chen, C., Mei, L., Xu, H., Wang, H., Zheng, Y., Liu, Z., Hong, J., Zhu, M., Qie, L., Zhang, L., Fan, C., and Guang, J.: A generalized land surface reflectance reconstruction method for aerosol retrieval: Application to the Particulate Observing Scanning Polarimeter (POSP) onboard GaoFen-5 (02) satellite, Remote Sens. Environ., 295, 113683, https://doi.org/10.1016/j.rse.2023.113683, 2023.

Stocker, T. F., Qin, D., Plattner, G.-K., Alexander, L. V., Allen, S. K., Bindoff, N. L., Bréon, F.-M., Church, J. A., Cubasch, U., and Emori, S.: Technical summary, in: Climate change 2013: the physical science basis. Contribution of Working Group I to the Fifth Assessment Report of the Intergovernmental Panel on Climate Change, Cambridge University Press, 33–115, 2013.

Sulla-Menashe, D. and Friedl, M. A.: User guide to collection 6 MODIS land cover (MCD12Q1 and MCD12C1) product, Usgs Rest. Va Usa, 1, 18, 2018.

Tegen, I.: Modeling the mineral dust aerosol cycle in the climate system, Quat. Sci. Rev., 22, 1821–1834, 2003.

Tørseth, K., Aas, W., Breivik, K., Fjæraa, A. M., Fiebig, M., Hjellbrekke, A.-G., Lund Myhre, C., Solberg, S., and Yttri, K. E.: Introduction to the European Monitoring and Evaluation Programme (EMEP) and observed atmospheric composition change during 1972–2009, Atmospheric Chem. Phys., 12, 5447–5481, 2012.

https://doi.org/10.5194/egusphere-2025-91
Preprint. Discussion started: 17 February 2025

Tummon, F., Solmon, F., Liousse, C., and Tadross, M.: Simulation of the direct and semidirect aerosol effects on the southern Africa regional climate during the biomass burning season, J. Geophys. Res. Atmospheres, 115, 2010.

Vellalassery, A., Pillai, D., Marshall, J., Gerbig, C., Buchwitz, M., Schneising, O., and Ravi, A.: Using TROPOspheric Monitoring Instrument (TROPOMI) measurements and Weather Research and Forecasting (WRF) CO modelling to understand the contribution of meteorology and emissions to an extreme air pollution event in India, Atmospheric Chem. Phys., 21, 5393–5414, 2021.

Virtanen, T. H., Kolmonen, P., Sogacheva, L., Rodríguez, E., Saponaro, G., and de Leeuw, G.: Collocation mismatch uncertainties in satellite aerosol retrieval validation, Atmospheric Meas. Tech., 11, 925–938, 2018.

Wang, Z., Ma, P., Zhang, L., Chen, H., Zhao, S., Zhou, W., Chen, C., Zhang, Y., Zhou, C., Mao, H., and others: Systematics of atmospheric environment monitoring in China via satellite remote sensing, Air Qual. Atmosphere Health, 14, 157–169, 2021.

Wei, J., Wang, J., Li, Z., Kondragunta, S., Anenberg, S., Wang, Y., Zhang, H., Diner, D., Hand, J., Lyapustin, A., Kahn, R., Colarco, P., Da Silva, A., and Ichoku, C.: Long-term mortality burden trends attributed to black carbon and PM2·5 from wildfire emissions across the continental USA from 2000 to 2020: a deep learning modelling study, Lancet Planet. Health, 7, e963–e975, https://doi.org/10.1016/S2542-5196(23)00235-8, 2023.

Wong, M. S., Nichol, J. E., and Lee, K. H.: An operational MODIS aerosol retrieval algorithm at high spatial resolution, and its application over a complex urban region, Atmospheric Res., 99, 579–589, 2011.

Wu, H., Tang, X., Wang, Z., Wu, L., Lu, M., Wei, L., and Zhu, J.: Probabilistic automatic outlier detection for surface air quality measurements from the China national environmental monitoring network, Adv. Atmospheric Sci., 35, 1522–1532, 2018.

Xian, D., Zhang, P., Gao, L., Sun, R., Zhang, H., and Jia, X.: Fengyun meteorological satellite products for earth system science applications, Adv. Atmospheric Sci., 38, 1267–1284, 2021.

Xie, G., Wang, M., Pan, J., and Zhu, Y.: Spatio-temporal variations and trends of MODIS C6.1 Dark Target and Deep Blue merged aerosol optical depth over China during 2000–2017, Atmos. Environ., 214, 116846, https://doi.org/10.1016/j.atmosenv.2019.116846, 2019.

Yuba, A., Huo, M., and Sato, K.: Global Atmosphere Watch (GAW) Aerosol Program, in: Handbook of Air Quality and Climate Change, Springer, 1–29, 2023.

Zhao, B., Jiang, J. H., Diner, D. J., Su, H., Gu, Y., Liou, K.-N., Jiang, Z., Huang, L., Takano, Y., and Fan, X.: Intra-annual variations of regional aerosol optical depth, vertical distribution, and particle types from multiple satellite and ground-based observational datasets, Atmospheric Chem. Phys., 18, 11247–11260, 2018.

Zhao, S., Wang, Q., Li, Y., Liu, S., Wang, Z., Zhu, L., and Wang, Z.: An overview of satellite remote sensing technology used in China's environmental protection, Earth Sci. Inform., 10, 137–148, 2017.